J. Xu et al. (Eds.)
© 2022 The authors and IOS Press.
This article is published online with Open Access by IOS Press and distributed under the terms of the Creative Commons Attribution Non-Commercial License 4.0 (CC BY-NC 4.0).
doi:10.3233/ATDE220207

Design and Laboratory Test of Vibration Excitation Device for Jujube Harvester

Zhiyuan ZHANG[a,b], Xianfei WANG[a,b] and Jingbin LI[a,b,1]
[a]*College of Mechanical and Electrical Engineering, Shihezi University, Shihezi,* 832003, *China*
[b]*Xinjiang Production and Construction Corps Key Laboratory of Modern Agricultural Machinery, Shihezi,* 832003, *China*

Abstract. In order to improve the working efficiency of excitation device of jujube harvester, an excitation device was designed by using eccentric block excitation mechanism. Through the combination of theoretical analysis and virtual simulation, the mass of eccentric block m, the motor speed n, the spring preload f were determined as test factors, and the angular acceleration α and amplitude A were used as evaluation indexes to carry out the combined test of orthogonal rotating center with three factors and five levels. First, this paper shows the maximum instantaneous angular acceleration α and the maximum amplitude A in space of the marking point of shift lever through 3D high-speed camera technology. Then, the Design-Expert v8.0.6.1 software was used for analysis of variance of experimental results, established the mathematical regression model of evaluation index and various relevant factors, and analyzed the influence of significant factors on evaluation index and optimized the test parameters. Final, the optimal parameters were determined as follows: eccentric mass m =233 g, motor speed n =1080 r/min, spring preload f =35 N. According to the combination of optimal parameters, the results shown that under the optimal combination of parameters, the average amplitude was A=46.73 mm, the average angular acceleration was α=11.72 rad/s^2, and the minimum inertia force generated by shell vibration was F=9.87 N. It could be seen that the excitation device satisfies the requirements for jujube harvesting. The study may provide theoretical basis and technical reference for the improvement of the excitation system of the jujube harvester.

Keywords. Jujube, harvester, motion simulation, amplitude, frequency

1. Introduction

Xinjiang is located in the hinterland of the Eurasian continent, which is a good place to breed high-quality jujube for its arid climate and abundant sunshine [1-3]. Statistics have shown that the total growing area of Xinjiang jujube reached 500,000 hm2 and 3,264,000 tons of jujube were produced by the end of 2017, making Xinjiang the biggest producer of jujube in China [4-5]. The booming of jujube in Xinjiang stimulated the market for jujube machine [6-7]. At present, Xinjiang jujube is mainly harvested by manual work. The low-efficiency and high-cost harvest method greatly restricted the sustainable development of Xinjiang jujube industry [8-9]. Hence, it is

[1]Corresponding Author, Jingbin LI, College of Mechanical Electrical Engineering, Shihezi University, Shihezi, China; Email: ljb8095@163.com.

urgent to realize mechanization to improve the efficiency and reduce the labor cost in jujube harvesting.

Jujube is an endemic species in China. The growing area and yield of jujube in China account for 99% of the whole world. So there are no mature jujube harvesting machine from other countries. But they have mature prototypes for other fruits e.g. citrus, mango, and apricot, etc. For example, Kececioglu developed a vibration harvester for olive harvesting. The harvester adopted eccentric block type excitation device to realize the harvesting. Researches have shown that the best harvesting happens at 20-28 Hz frequency and 10s vibrating at 20-30 mm amplitude [10]; Donald and Stephen designed an apple harvester which shakes the tree trunk with an eccentric block type excitation device. Researches showed that the average classification rate of the harvester is 87% when working, and the average vibration harvest rate is more than 95% [11]; Parameswarakumar and Gupta designed an inertial type slider-crank mango harvester which adopted branch shaking method for mango harvesting. Researches showed that the highest harvest rate can be achieved when the frequency is at 11-13 Hz and the amplitude is 76-102 mm. At this time, the damage to the fruit tree is also the smallest [12]. Wang Changqin and Xu Linyun et al. studied a shaking type fruit harvester, which adopted symmetrically placed eccentric block for the excitation device. The test on harvesting walnut showed that the average harvesting rate reached 89.5%-92.6% when the excitation frequency is 19-20 Hz, and no destructive damage on the trunk from the clamping device was found [13-14]; A 4YS-24 type jujube harvester was developed in the Institute of Machinery Equipment, Xinjiang Academy of Agricultural and Reclamation Science. This harvester also adopted the shaking harvest mode. The vibration exciter used an eccentric block to generate omnidirectional vibration. Tests showed that the harvest clean rate is as high as 91.4% for jujube trees with trunk diameter between 80-200 mm and growing row spacing of more than 4 m [15-16]; based on the dwarf and close planting mode of Xinjiang jujube, College of Mechanical and Electrical Engineering of Shihezi University developed a crown vibration-based all-hydraulic and self-propelled jujube harvester using slider-crank mechanism as the excitation source. The initial amplitude of the vibration dial is 15-20 mm, the excitation frequency is 15-20 Hz, and the harvest rate is 90% [17].

Above all, there are mainly two types of fruit harvester excitation device: eccentric action type excitation device, and fixed route slider-crank excitation device[18]. The first type generates inertial centrifugal force through the uniform circular movement of the eccentric block and makes reciprocated excitations under the effect of the inertial centrifugal force. The device is featured with simple structure, high vibration frequency and large exciting force. But eccentric block is required and needs to be changed when adjusting amplitude in this mechanism. Therefore, the device is mainly used for large harvesting machinery [19-20]; the later type called the slider-crank excitation device rotates the crank to drive the output rod and makes straight reciprocating movement. This device can realize a wide route but cannot make adjustment according to the characteristics of the harvesting target, which may harm the fruit tree [21-22].

Based on previous researches on the effect of jujube tree excitation transfer and considering the high cost and low efficiency in Xinjiang jujube harvesting, this paper designed an excitation device for large jujube harvester. The excitation device used three eccentric blocks for the source. The paper mainly studied the eccentric mass, speed and the effect of damping device's spring preload on the amplitude and angular acceleration, and laboratory tests were also conducted. The research can provide theoretical basis and technical support for the design of excitation device of jujube harvester.

2. Structure and working principle

2.1. Structure

The eccentric block type vibrator mainly consists of excitation device, rotary roller and damping device. The excitation device is made up of shell, timing pulley, timing belt, revolution axis, rotation axis, and three evenly placed eccentric blocks with equivalent mass; the rotary roller is composed by roller assembly and dial; the damping device includes the spring, damper belt and damper wheel; the excitation device and rotary roller are fixed by flange, the rotary roller and the damping device are fixed and connected by flat key, and the vibrator is fixed to the rack by two vertical plummer blocks. Fig. 1 showed the schematic of the vibrator.

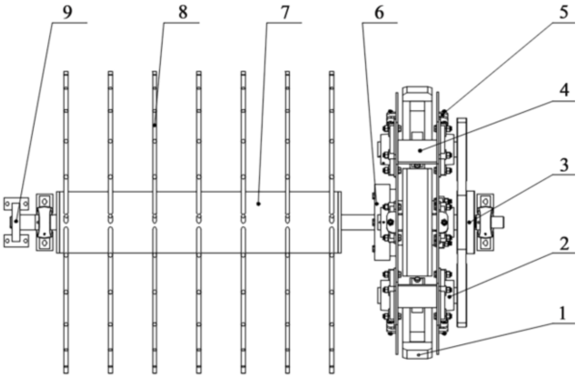

1. Eccentric block 2. Bearing seat 3. Synchronous pulley 4. Housing 5. Adjusting sheet 6. Flange 7. Rotating drum 8. Paddle 9. Damping device

Figure 1. The schematic of the vibrator.

2.2. Working principle

The eccentric block type vibrator, which is driven by hydraulic motor, is the major part of a jujube harvester. When working, the hydraulic motor drives the revolution axis and the timing pulley on the revolution axis to rotate; then the timing pulley will drive the three evenly placed eccentric blocks to rotate at a constant angular velocity; the rotating eccentric blocks will produce centrifugal force and further generate couple moment to drive the shell and rotary roller to make reciprocated rotation. Therefore, the device can adjust the motor speed to control the amplitude and frequency of the rotary roller and realize a high-frequency and small-amplitude harvesting of jujube.

3. Motion and vibration analysis of excitation device

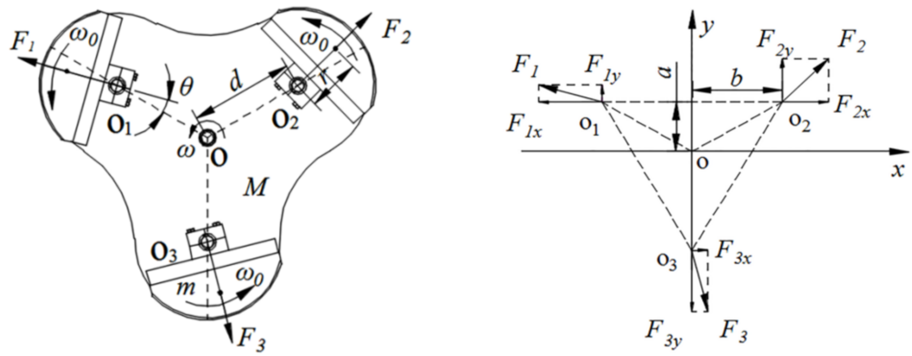

a Excitation device motion analysis diagram

b Inertial centrifugal force decomposition diagram

Figure 2. Excitation device motion analysis.

The power source of the excitation device comes from three synchronously rotated eccentric blocks (angular velocity=ω_0) which generate a centrifugal force F on the shell through the rotation axis O_1, O_2 and O_3, then the couple on the shell will actuate the vibration of the rotary roller around the revolution axis O. In order to simplify the excitation device, the rotary roller and the shell were rolled up into one. The motion model is shown as Fig. 2.

Fig. 2a is the simplified model of the excitation device and Fig. 2b is the force diagram of the excitation device; k is the elastic coefficient; c is the damping coefficient; m is the mass of the eccentric, g; M is the mass of the shell and rotary roller device (hereafter referred to as shell), g; d is the distance between the eccentric axis's rotation axis and the revolution axis, mm; r is the distance between eccentric mass center and rotation axis, mm; R is the radius of the shell, mm; ω_0 is the eccentric block rotation angular velocity, rad/s; ω is the angular velocity of the vibration of the shell and rotary roller device, rad/s; θ is the angle that the eccentric block rotates around the rotation axis, rad; φ is the rotation angle of the eccentric axis's rotation axis around the revolution axis，rad; F is the inertial centrifugal force generated by the rotation of the eccentric block, N.

3.1. Excitation device motion analysis

When the excitation device is working, the eccentric blocks rotate at the angular velocity of ω_0 at time t; the rotation angle of the eccentric blocks is θ, and the rotation angle of the shell is φ, which means,

$$\theta=\omega_0 \cdot t \tag{1}$$

$$\varphi=\omega \cdot t \tag{2}$$

where, t is the time, s; F is the inertial centrifugal force produced by the rotation of the eccentric blocks, N; then

$$F = m \cdot r \cdot \omega_0^{\,2} \tag{3}$$

The three working eccentric blocks have the same inertial centrifugal force F because they have the same mass, geometric dimensioning and rotating angular velocity, then,

$$F_1 = F_2 = F_3 = F \tag{4}$$

where, F_1, F_2 and F_3 represent the inertial centrifugal forces of three eccentric blocks rotating the rotation axis O_1, O_2 and O_3, respectively. When the relative position of the three eccentric blocks with the shell is the same as the Fig. 2a, the Cartesian coordinate system O-xy was established. The inertial centrifugal force decomposition diagram of this system is shown as Fig. 2b. At this time, F_1, F_2 and F_3 can be decomposed into F_{1x}, F_{2x} and F_{3x} in the x-axis direction and F_{1y}, F_{2y} and F_{3y} in the y-axis direction. Then we sum the component forces in both the x-axis and y-axis:

$$\begin{cases} F_x = F_{1x} + F_{2x} + F_{3x} = 0 \\ F_y = F_{1y} + F_{2y} + F_{3y} = 0 \end{cases} \tag{5}$$

According to (5), the joint inertial centrifugal force produced by the eccentric blocks is 0 N; then we calculated the couples on the revolution axis for the composition forces of each inertial centrifugal force respectively (ω direction is the positive direction), and we can get:

$$\sum M_O(F) = F_{1x} \cdot a - F_{1y} \cdot b - F_{2x} \cdot a + F_{2y} \cdot b + F_{3x} \cdot d \tag{6}$$

where, a and b stand for the distance, m; according to the triangle relationship in Fig. 2b, we can get:

$$a = \frac{1}{2} \cdot d\,,\quad b = \frac{\sqrt{3}}{2} \cdot d \tag{7}$$

Combine (4), (6) and (7):

$$\sum M_O(F) = {}^{5}\!/_{2} \cdot d \cdot F \cdot \sin\theta \tag{8}$$

The analysis of (8) showed that the motion law of the shell satisfies the simple harmonic motion under the effect of driving couple moment. When $\theta \in (0,\ \pi)$, the driving couple moment drives the shell in the anti-clockwise direction to enable the shell's anti-clockwise acceleration vibration; when $\theta \in (\pi,\ 2\pi)$, the driving couple moment drives the shell in the clockwise direction to enable the shell's anti-clockwise reduction vibration.

3.2. Vibration analysis of excitation device

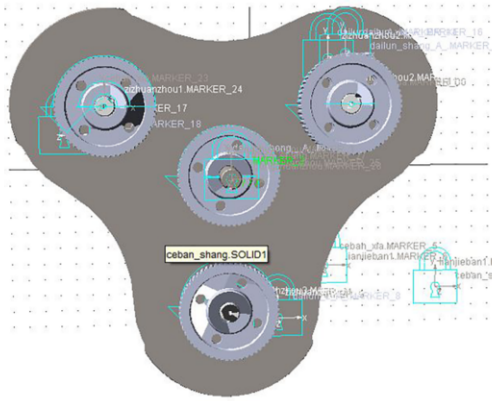

Figure 3. Vibrator simulation analysis

In order to verify the correctness of the theoretical analysis, the simplified model is drawn by SolidWorks software as the simulation model, saved as *.x_t format and imported into ADAMS software. The male rotating shaft is connected with the ground as a fixed pair, and a rotating pair is added between the male rotating shaft and the shell, and between the shell and their respective rotating shafts. The motion simulation of the device is carried out, as shown in Fig. 3. The simulation mainly analyzes the motion state of the simplified excitation device shell, where M=100 kg, m=10 kg, d=0.28 m, r=0.12 m, ω_0=3 rad/s, set the simulation time to 5 s, and obtain the time-varying curves of angular velocity and angular acceleration of shell and synchronous pulley, as shown in Fig. 4.

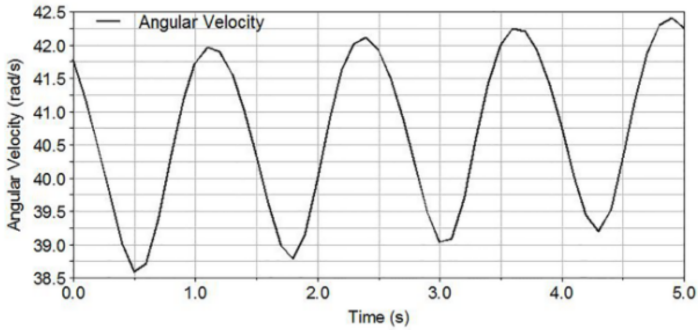

a Curve of angular velocity of shell motion with time

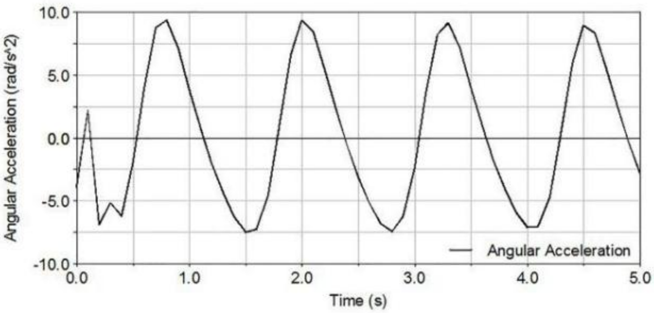

b Curve of angular acceleration of shell motion with time

Figure 4. The simulation of angular velocity and angular acceleration with time.

From the angular velocity and angular acceleration curves of ADAMS software simulation diagram, it can be seen that in the time period of 1.2 s, the motion curve is a regular simple harmonic curve, and the angular velocity increases with the increase of angular acceleration, but when the angular acceleration is maximum, the angular velocity does not reach the maximum value. In Fig. 4, it can be seen from the angular velocity diagram that the angular velocity value at the wave crest is gradually increasing because the vibration exciter damping device is ignored in the simulation; The stiffness coefficient and damping coefficient of the damping device have obvious influence on the diagonal velocity curve and angular acceleration curve, which proves the rationality of the vibration exciter design of the damping device. Therefore, the curve obtained from the motion analysis of ADAMS software is basically consistent with the curve derived from the theoretical formula.

3.3. Vibration analysis of excitation device

Apply conservation law of mechanical energy to the system:

$$W = T + U + V \tag{9}$$

where, W is the couple work of the inertial centrifugal force, J; T is the kinetic energy, J; U is the elastic potential energy, J; V is the Rayleigh dissipates energy, J.

Then the couple work of the inertial centrifugal force W is:

$$W = \sum M_O(F) \cdot \beta = {}^{5}\!/_{2} \cdot d \cdot F \cdot \sin\theta \cdot \varphi \tag{10}$$

The kinetic energy T of the system produced during vibration is:

$$T = {}^{3}\!/_{2} \cdot J_0 \cdot \omega^2 + {}^{1}\!/_{2} \cdot J_k \cdot \omega^2 \tag{11}$$

where, J_0 and J_k are the moments of inertia of the eccentric block and the shell, kg·m^2; the moments of inertia J_0 and J_k of the eccentric block and the shell on the revolution axis O are:

$$\begin{cases} J_0 = m \cdot r^2 + m \cdot R_c^2 \\ J_k = 1/2 \cdot M \cdot R^2 \end{cases}$$

Where, R_c is the distance from the eccentric mass center to the revolution O, mm;

$$R_c = \sqrt{d^2 + r^2 + 2 \cdot d \cdot r \cos\theta}$$

The spring preload of the damping device is f, N; then $f = k \cdot \Delta x$

The elastic potential energy U produced from the damping spring during the vibration of the system is:

$$\mathrm{U} = 1/2 \cdot k \cdot (x + \Delta x)^2 + 1/2 \cdot k \cdot (x - \Delta x)^2 = k \cdot \Delta x^2 = f \cdot \Delta x \quad (12)$$

where x and Δx are the original length and elongation of the damping spring, m; k is the spring stiffness factor, N/m; $\Delta x = \varphi \cdot R$.

During the vibration, the Rayleigh dissipates energy V produced from the damping device is:

$$\mathrm{V} = 1/2 \cdot c \cdot \dot{\varphi}^2 = 1/2 \cdot c \cdot \omega^2 \quad (13)$$

After combining the above formulas and ignoring the Rayleigh dissipates energy V, we can get the angular acceleration of the shell α:

$$\alpha = \frac{2 \cdot f \cdot R + 5 \cdot d \cdot m \cdot r \cdot \omega_0{}^2 \cdot \sin(\omega_0 \cdot t)}{3J_0 + J_k} \quad (14)$$

The accelerated velocity of the shell vibration is a, m/s^2, and:

$$a = \alpha \cdot R \quad (15)$$

According to (14), the shell can make reciprocating movement during the vibration; tests showed that the maximum breaking force of jujube handle is 6 N [3-4]. By combining (15) and $F = Ma$ (M is the shell mass, g; a is the acceleration of the shell vibration, m/s2) we can calculate the inertia force applied on the shell from the stimulation of the eccentric blocks and judge whether the eccentric device test-bed can satisfy the work requirement.

4. Test materials and methods

4.1. Test materials

Test device: eccentric block excitation device; test field: Xinjiang Production and Construction Corps Key Laboratory of Modern Agricultural Machinery, Shihezi University.

4.2. Test methods

This test studied the influencing factors to the vibration effect based on the structure and changing of working parameters of the excitation device.

4.2.1. Determination of influencing factors

According to the motion analysis, structure parameters and working parameters of the excitation device, this test selected three major influencing factors (eccentric mass *m*, damping spring preload *f*, and motor speed *n*) that influence the vibration effect of the excitation device.

(1) Eccentric mass

Eccentric mass has a direction effect on the working effect of the excitation device. According to (16) and (17), higher eccentric mass will cause larger inertia couple moment and angular acceleration and create better vibration effect of the excitation device. The study set the eccentric mass *m* at 198-242 g according to the jujube harvesting requirement, and the working condition and reliability of the testing apparatus.

$$\sum M_O(F) = {}^5\!/_2 \cdot d \cdot F \cdot \sin\theta = {}^5\!/_2 \cdot d \cdot m \cdot r \cdot \omega_0^{\,2} \cdot \sin\theta \tag{16}$$

$$\alpha = \frac{2 \cdot f \cdot R + 5 \cdot d \cdot m \cdot r \cdot \omega_0^{\,2} \cdot \sin\left(\omega_0 \cdot t\right)}{3J_0 + J_k} \tag{17}$$

(2) Motor speed

Motor speed *n* has a direct impact on the angular velocity *ω0* of three eccentric blocks rotating their own rotation axis. Formula (17) showed that the maximum angular acceleration *α* has a direction connection with *ω0*; the relationship between motor speed *n* and the angular acceleration of the eccentric block is: $n = {}^{\pi\omega_0}\!/_{30}$, where *n* is the speed, r/min; *ω0* is the angular velocity, rad/s; based on previous researches [4], the motor speed can be set at 960-1080 r/min when the resonant frequency of the sample jujube tree is 13-18 Hz.

(3) Spring preload

The damping spring preload *f* has a large impact on the dial vibration of the excitation device. The larger the preload, the smaller the amplitude will be. According to (17), the larger the *f*, the larger the angular acceleration *α* will be; previous pre-test showed that the best effect can be achieved when the damping spring preload f=25-45 N.

4.2.2. Determination of response indexes

This test employed 3D high-speed photograph technology and 3D ProAnalyst software to measure the response indexes of maximum amplitude A and maximum angular acceleration α of the top dial point of the excitation device under different working parameters. The spatial motion trail, amplitude and angular acceleration of the test-bed and dial point are shown as Fig. 5.

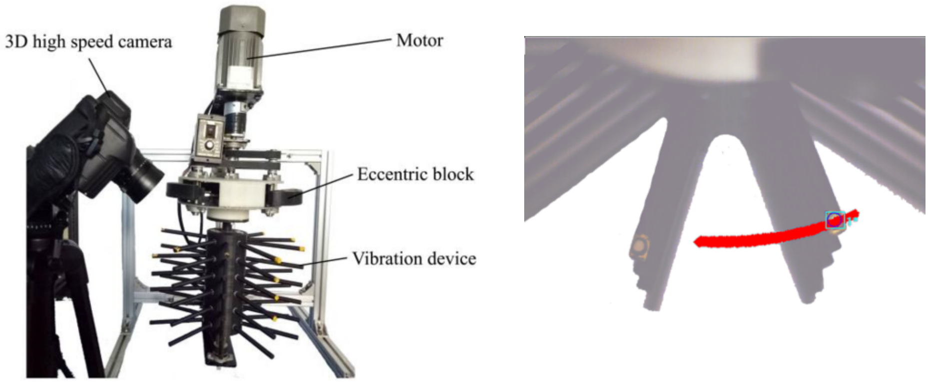

a. The test-bed of excitation device b. The motion trajectory of marker point

Figure 5. The motion analysis of device.

(1) Maximum amplitude

The amplitude of the excitation device has a large impact on the working effect of the vibrator. The larger the amplitude, the better the vibration effect will be. With dial's maximum amplitude A as the response index, we used 3D ProAnalyst to analyze the dial's spatial motion trail which was photographed by 3D high-speed camera, and then we confirmed the maximum amplitude A of the dial in this section by statistical analysis.

(2) Maximum angular acceleration

According to (17), the maximum angular acceleration α of the dial is closely related to the eccentric mass m, damping spring preload f, and motor speed n. With dial's maximum angular acceleration α as the response index, we used 3D ProAnalyst to analyze the dial's spatial motion trail which was photographed by 3D high-speed camera and we got the maximum angular acceleration α.

When using 3D ProAnalyst to conduct the test analysis, we selected a section of stable vibration (about 500 frames) as the test data collection samples, and confirmed the maximum amplitude A and maximum angular acceleration of the dial in this section by statistical analysis.

4.2.3. Design of test

This test used Design-Expert V8.0.6.1 to make an optimal three-factor and five-level orthogonal rotation center combination test. The eccentric mass m, motor speed n, and damping spring preload f were also studied. The test factors and levels are shown as Table 1.

Table 1. Factors and levels of exciter test.

Level	Factor		
	Eccentric mass *m*/g	**Motor speed *n*/(r/min)**	**Spring preload *f*/N**
Upper asterisk arm(1.682)	242	1121	52
Upper level(1)	233	1080	45
Zero level(0)	220	1020	35
Lower level(-1)	207	960	25
Lower asterisk arm(-1.682)	198	919	18

5. Results and analysis

5.1. Regression analysis of test results

This test is divided into 20 groups, and each group was repeated five times. The average of the five tests was taken as the final test result, shown as Table 2.

Table 2. Experiment design and results.

No.	Factors and levels			Response index	
	X_1/g	X_2/(r/min)	X_3/N	Y_1/mm	Y_2/(rad/s^2)
1	207	960	25	109.72	7.93
2	233	960	25	179.77	9.79
3	207	1080	25	61.01	9.4
4	233	1080	25	112.89	10.15
5	207	960	45	92.67	9.01
6	233	960	45	156.98	10.95
7	207	1080	45	55.01	10.56
8	233	1080	45	29.56	12.84
9	198	1020	35	50.42	8.77
10	242	1020	35	158.85	12.15
11	220	919	35	145.21	8.78
12	220	1121	35	56.19	11.03
13	220	1020	18	98.9	8.63
14	220	1020	52	49.65	11.19
15	220	1020	35	74.85	9.83
16	220	1020	35	76.47	10.24
17	220	1020	35	66.97	10.11
18	220	1020	35	76.8	9.62
19	220	1020	35	61.24	10.22
20	220	1020	35	59.95	10.12

Note: X_1 is eccentric mass, g; X_2 is motor speed, r/min; X_3 is spring preload, N; Y_1 is amplitude, mm; Y_2 is angular acceleration, m/s^2.

Then a variance analysis was conducted using Design-Expert V8.0.6.1, and the coding regression mathematical models, which took dial's maximum amplitude A and maximum angular acceleration α as the response functions respectively and each influencing factor as the independent variable, were established, as shown in Formula (18) and Formula (19).

$$Y_1 = 71.51 + 25.13 \cdot X_1 - 31.51 \cdot X_2 - 15.52 \cdot X_3 - 13.49 \cdot X_1 \cdot X_2 - 10.38 \cdot X_1 \cdot X_3 + 13.25 \cdot X_1^2 + 11.86 \cdot X_2^2 \tag{18}$$

$$Y_2 = 9.96 + 0.92 \cdot X_1 + 0.66 \cdot X_2 + 0.76 \cdot X_3 + 0.2 \cdot X_1 \cdot X_3 + 0.2 \cdot X_2 \cdot X_3 + 0.16 \cdot X_1^2 \tag{19}$$

where, X_1, X_2 and X_3 stand for the eccentric mass *m*, motor speed *n* and spring preload *f*.

The regression analysis results in Table 3 showed that the equation evaluation indexes of amplitude *A* and *P* value of angular acceleration *α* are all smaller than 0.01, which means the result of the regression equation model in (17) and (18) is significant. Meanwhile, the determination coefficients R^2 are 0.9485 and 0.9342 respectively, which indicated that the two models can fit over 93% of the test results. Therefore, the above two regression equations have a good fitting relationship with the real situations, which is of practical significance.

Table 3. Variance analysis of regression models.

Experimental index	Difference source	Sum of squares	Degree of freedom	Mean square	*F* value	*P* value
Amplitude/mm	Model	32020.23	7	4574.32	25.19	< 0.0001(**)
	Residual	2179.10	12	181.59		
	Lake of Fit	1882.86	7	268.98	4.54	0.0575
	Purea Error	296.24	5	59.25		
Angular Acceleration/(m/s^2)	Model	26.40119	6	4.400199	74.43519	< 0.0001(**)
	Residual	0.768488	13	0.059114		
	Lake of Fit	0.465955	8	0.058244	0.962611	0.5433
	Purea Error	0.302533	5	0.060507		

Note: P<0.01(highly significant,**);P<0.05(significant,*); P>0.05(not significant)

5.2. Influence of test factors on amplitude

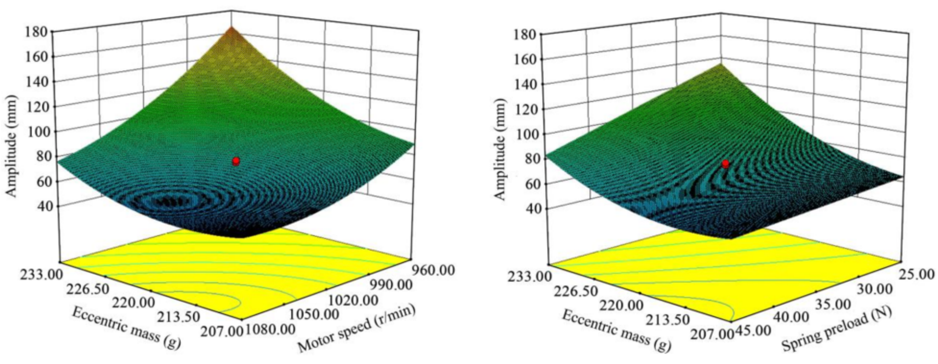

a. Effect of eccentric mass and motor speed on amplitude, while spring preload is 35 N

b. Effect of eccentric mass and spring preload on amplitude, while motor speed is 1020 r/min

Figure 6. Effect of experiment factors on amplitude.

The 3D response surface diagram of eccentric mass *m*, motor speed *n* and spring preload *f* on the amplitude *A* is shown as Fig. 6a-6b. In Fig. 6a, when the spring preload *f* is at the 0 level (*f* =35 N), the law of the interaction influencing the amplitude *A* is as follows: the amplitude *A* increased slowly with the eccentric mass *m* while decreased rapidly with the motor speed *n*, showing that, under test level, the effect on the amplitude *A* from motor speed *n* is more significant than that from eccentric mass *m*. In Fig. 6b, when the motor speed *n* is at the 0 level (*n* =1020 r/min), the law of the interaction influencing the amplitude *A* is as follows: the amplitude *A* increased rapidly with the eccentric mass *m* while decreased slowly with the spring preload *f*, showing that, under test level, the effect on the amplitude *A* from eccentric mass *m* is more significant than that from spring preload *f*.

Therefore, the order of the significance of interaction influencing the amplitude *A* under test level is: motor speed *n*>eccentric mass *m*> spring preload *f*.

5.3. Effect of test factors on angular acceleration

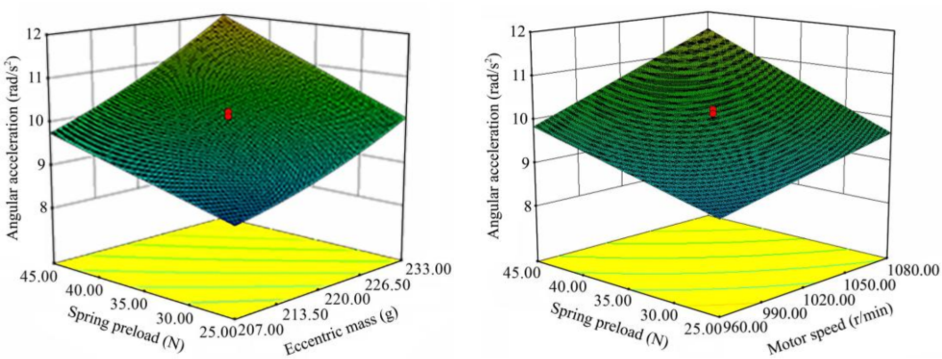

a. Effect of spring preload and eccentric mass on angular acceleration, while motor speed is 1020 r/min

b. Effect of spring preload and motor speed on angular acceleration, while eccentric mass is 220 g

Figure 7. Effect of test factors on angular acceleration.

The 3D response surface diagram of eccentric mass *m*, motor speed *n* and spring preload *f* on the angular acceleration *α* is shown as Fig. 7a-7b. In Fig. 7a, when the motor speed *n* is at the 0 level (*n*=1020 r/min), the law of the interaction influencing the angular acceleration *α* is as follows: the angular acceleration *α* increased rapidly with the spring preload *f* and the eccentric mass *m,* while the interaction between eccentric mass *m* and angular acceleration *α* is more obvious. This shows that, under test level, the effect on the angular acceleration *α* from eccentric mass *m* is more significant than that from spring preload *f*. In Fig. 7b, when the eccentric mass *m*, is at the 0 level (*m*=220 g), the law of the interaction influencing the angular acceleration *α* is as follows: the angular acceleration *α* increased with the spring preload *f* and the motor speed *n*, but the change of the motor speed *n* is larger than the change of the spring preload *f* on the angular acceleration *α*, which shows that, under test level, the effect on the angular acceleration *α* from motor speed *n* is more significant than that from spring preload *f*.

Therefore, under test level, the effect from the eccentric mass m on the angular acceleration α is the most significant, followed by motor speed n and spring preload f.

5.4. Parameters optimization and verification

5.4.1. Parameters optimization

In order to further optimize the structural parameters and working parameters of jujube harvest vibrator and get the optimal combination of parameters, this paper made an optimization on the test device based on the requirement of high-frequency and small-amplitude jujube harvesting [31-32]. Design-Expert V8.0.6.1 was used to make an optimal analysis on the 3-index quadratic regression model. The constraints include: 1) Objective function: A[min]; α[max]; 2) Influencing factor constraints: $m\in[-1,1]$ (eccentric mass 207-233 g); $n\in[-1,1]$ (motor speed 960-1080 r/min); $f\in[-1,1]$ (spring preload 25-45 N). After optimization, the Design-Expert V8.0.6.1 was used to choose the combination with the highest satisfaction degree as the optimal parameter combination: eccentric mass m=233 g, motor speed n=1080 r/min, spring preload f=35 N, model predicted amplitude A=50 mm, and angular acceleration α=13 rad/s^2.

5.4.2. Test verification

The test was conducted on the test-bed of the excitation device. Parameter combination: eccentric mass m=233 g, motor speed n=1080 r/min, spring preload f=35 N. The test showed that the test-bed shell mass M=3000 g, shell radius R=0.3 m, and the vibration acceleration of the shell can be obtained by $a=\alpha\cdot R$. The test was conducted five times and the average of the five tests was taken as the final test result (Table 4).

Table 4. Measurement results of test-bed testing.

	Max	Min	Avg.	S.D.	C.V.
Amplitude/mm	51.21	42.32	46.73	3.63	7.78%
Angular acceleration/(rad/s^2)	12.33	10.96	11.72	0.61	5.13%
Acceleration/(m/s^2)	3.70	3.29	3.51	0.18	5.13%

The test-bed testing using the optimal parameter combination is shown in Table 4. As shown, the average amplitude A=46.73 mm, and the average angular acceleration α=11.72 rad/s^2, which were lower than expected. The reason is due to the processing errors of the test-bed; through $F=Ma$ (M is the shell mass, and a is the vibration acceleration of the shell), we calculated the minimum inertial force imposed on the shell from the eccentric block excitation F=9.87 N, which is larger than the maximum breaking force of the jujube handle (6 N), showing that this excitation device can satisfy the requirement of jujube harvesting.

6. Conclusion

(1) This paper designed a excitation device used in large jujube harvester to deal with the current high-cost and low-efficiency harvesting of Xinjiang jujube. The excitation device is powered by three eccentric blocks, which can realize a continual work of the harvester;

(2) Based on the kinematic analysis of the excitation device, we worked out the relationship between the angular acceleration α and the eccentric mass m, motor speed n, and spring preload f;

(3) Through response surface tests, we analyzed the effect trend of eccentric mass m, motor speed n and spring preload f on the amplitude A and angular acceleration α, and established a quadratic multiple response model of amplitude A and angular acceleration α on the three factor levels; the order of the significance of each test factors influencing the amplitude A is: motor speed n, eccentric mass m, and spring preload f, successively; under test level, the effect from the eccentric mass m on the angular acceleration α is the most significant, followed by motor speed n and spring preload f;

(4) Design-Expert V8.0.6.1 is used to optimize the test results, and the optimal parameter combination is: eccentric mass m=233 g, motor speed n=1080 r/min, spring preload f=35 N;

(5) According to the test based on the optimal parameter combination, the average amplitude A=46.73 mm, average angular acceleration α=11.72 rad/s^2, and the minimum iner.tial force imposed on the shell from the eccentric block excitation F=9.87 N, which showed that this excitation device can satisfy the requirement of jujube harvesting.

References

[1] Rendong S, Tingting Q, Qqinbo Z, Anyan C, Wei Z, Shenduo L, Caiqi H. Design of Jujube Harvester Based on Hydraulic Driven. Journal of Qingdao Agricultural University (Natural Science). 2020 Nov; 37(3): pp 230-234.

[2] Yuanhang Z, Za K, ChengSong L, Huiming Z, Wei F, Jian C. Research and development of fruit collection techniques for landing fruit trees. Journal of A gricultural Mechanization Research. 2017 Jan; 39(1): pp 256-263.

[3] Fengkui Z, Fufeng Y, Zzhongjie L, Hong Z, Haipeng L, Ping L, Chaojun Z. Design and field testing of the air-suction machine for picking up Chinese jujube fruits. Journal of Fruit Science. 2019 Dec; 37(2): pp 278-285.

[4] Wei F, Zhiyuan Z, Yudong L, Junbing P, Jian C, Kai D, Huiming Z. Simulation Experiment in Lab on Force Transfer Effect of Jujube under Excitation. Transactions of the CSAE. 2017 Sep; 33(17): pp 65-72.

[5] Xiaocheng G, Qian'e L. Jujube Cultivation Techniques. Yangling, Shaanxi: Northwest A&F University Press; 2005.

[6] Can H, Bing L, Shulin H, Xiaokang Y, Xufeng W. Research status and development countermeasures on harvesting machinery of jujube in Xinjiang. Journal of Chinese Agricultural Mechanization. 2016 Jul; 37(7): pp 222-240.

[7] Gaokun S. Design and experimental study of pneumatic red dates harvesting machinery. Alar: Tarim University; 2014 Jun.

[8] Yaou Z, Za K, Chengsong L, Wei F, Lihong W, Linlin L. Design of Dwarf and Close Planting Jujube Harvester Pickup Device. Journal of Agricultural Mechanization Research. 2016 Apr; 38(4): pp 71-75.

[9] Junbing P, Yudong L, Kai D, Zhiyunan Z, Wei F. Design and Motion Simulation of Pneumatic Device for Picking up Ground Jujube. Journal of Agricultural Mechanization Research. 2018 Feb; 40(09): pp 139-143.

[10] Kececioglu. Atalet kuvvet tipli sarsici ile zeytin hasadi imkanlari uzerine bir arastirma (Research on olive harvesting possibilities with an inertia type shaker). Izmir, Turkey: Department of Agricultural Machinery, Agricultural Faculty, Ege University; 1975.

[11] Donald Peterson L, Stephen Miller S. Advances in Mechanical Harvesting of Fresh Market Quality Apples. Journal of Agricultural Engineering Research.1989 Jan; 42(01): pp 43-50.

[12] Parameswarakumar M, Gupta CP. Design Parameters for Vibratory Mango Harvesting System. Transactions of the ASAE. 1991 Jan; 34(1): pp 14-20.

[13] Changqin W, Linyun X, Hongping Z, Yeming C, Hua C. Development and experiment of eccentric-type vibratory harvester for forest-fruits. Transactions of the CSAE. 2012 Aug; 28(16): pp 10-16.
[14] Changqin W. Design and Experimental Study of the Eccentric-type Forest-fruit Vibratory Harvester. Nanjing: Nanjing Forestry University; 2012 Jun.
[15] Zhihui T, Xiangjin M, Congju S, Shouxing J, Yan Z, Xuan Z, Chaoming Q. Design and Experimental Investigation of Mechanical Vibration Tree Fruits and Nuts Harveste. Journal of Agricultural Mechanization Research. 2010 Aug; 32(8): pp 65-69.
[16] Zhihui T, Xiangjin M, Congju S, Shouxing J, Yan Z, Xuan Z, Qiwei C, Liqaing Y. Development of 4YS-24 type jujube harvester. Xinjiang Agricultural Mechanization; 2010 Feb; (1): pp 30-32.
[17] Rong H, Za K, Wei F, Lihong W, Hongyin Y, Yu S, Shizhe C. Design and Kinematic Analysis of Excitation Device of Dwarf and Close Planting Jujube Harvest Machine. Journal of Agricultural Mechanization Research. 2014 Feb; 36(02): pp 64-67.
[18] Luhong T, Yimunisha A, Ying D. Power harvesting of fruit trees in foreign countries. Xinjiang Agricultural Mechanization. 2004 Jun; (3): pp 54-56.
[19] Li GY. Selection and Calculation of Vibration Parameters of Vibratory Seed Seeder. Journal of Nanjing Forestry University (Nat. Sci. Ed.). 1984 Apr; 8(1): pp 101-114.
[20] Lenker DH, Hedden SL. Optimum shaking action for citrus fruit harvesting. Transactions of the ASAE. 1968 Jan; 11(3): pp 347-349.
[21] Peterson DL, Wolford SD. Mechanical harvester for fresh market quality stemless sweet cherries. Transactions of the ASAE. 2001 Jan; 44(3): pp 481-485.
[22] Liang Y,Yin LQ. Experimental Research on Harvesting Seabuckthorn Vibrator. The Global Seabuckthorn Research and Development. 2009 Dec; 6(4): pp 32-38.